The Spatial Statistics of Structural Magnetic Resonance Images: Application to Quality Assessment of Brain MRI Images

Michael Osadebey, Marius Pedersen, Douglas Arnold, and Katrina Wendel-Mitoraj, The Alzheimer's Disease Neuroimaging Initiative*

Abstract

Popular algorithms for quality evaluation of medical images are generic, global and distortion-specific. Performance is limited by complexity introduced by presence of disease signatures such as lesions. Application of classical statistics ignores spatial dependency and the unique image attributes in different imaging modalities. We propose a new no-reference method that overcomes some draw-backs of current algorithms and correlate with human visual system in terms of 'fidelity', 'usefulness' and 'naturalness'. We define the sample space as local entropy at pixel locations in a MRI volume data. Furthermore we segment each slice into eight equal angular segments and partition the sample space into low and high entropy regions. These regions, in a MRI volume data, are regarded as regionalized random variables which exhibit distinct and organized geographic patterns. Our proposal has 'usefulness' because it exploits similarity in geometry of human anatomy to build quality models from 250 brain MRI images of different subjects sourced from the Alzheimer's disease neuroimaging initiative (ADNI) database. 'Fidelity' is impacted by comparing quality models built from ADNI images with quality features extracted from a test image. 'Naturalness' comes from application of spatial statistics to describe distinct geographic patterns of different anatomic structures of brain. Quality scores computed using law of total probability takes into account presence of lesions in MRI data. Partition of feature space encourages focus on region of interest. Experimental results show that our proposal correlates with different levels of degradation and can improve discernment of a physician or a trained reader towards reliable diagnosis.

Index Terms

Magnetic Resonance Imaging, Image Quality, Quality Feature, Quality Score, Total Probability, Semivariogram and Gaussian Distribution

I. INTRODUCTION

EVALUATION of image quality is a preliminary post-acquisition step. The quality of image acquisition devices, the necessary post-acquisition processing procedures, performance evaluation of image processing and image analysis algorithms and the level of utility of an image is determined by the outcome of image quality evaluation. Strategic imaging work-flow decisions such as choice of imaging device, algorithms for image processing and image analysis, re-scan, re-processing and re-analysis are influenced by image quality evaluation. The extent to which a trained reader or an automated image analysis system can optimally extract the information contained in an image is determined by the image quality. Thus image quality assessment is a very important step in the process of utilization of an image.

M. Osadebey is with NeuroRx Research Inc, 3575 Parc Avenue, Suite # 5322, Montreal, QC, H2X 3P9, Canada e-mail: mosadebey@neurorx.com.

M, Pedersen is with the Faculty of Computer Science and Media Technology, NTNU - Norwegian University of Science and Technology, Gjovik, Norway email: marius.pedersen@ntnu.no.

D, Arnold is with NeuroRx Research Inc, 3575 Parc Avenue, Suite # 5322, Montreal, QC, H2X 3P9, Canada e-mail: douglas.arnold@mcgill.ca.

K, Wendel-Miitoraj is with BrainCare Oy, Niemenmaantie 30, 33960 Pirkkala, Finland, e-mail: katrina@braincare.fi.

The first step in the evaluation of image quality is the identification of manageable image quality attributes [1], [2]. These attributes expressed as quality features are then measured using different quality scores to obtain a total quality score referred to as image quality index [3]. The goal of objective image quality evaluation is to derive an image quality metric which correlates with the evaluation by the human visual system in terms of 'fidelity', 'usefulness' and 'naturalness' [4]. Image quality can be evaluated by humans in what is referred to as subjective method or by a measuring device in what is referred to as objective method. This paper focus on how to quantify the diagnostic information contained in structural magnetic resonance images of the brain without reference to an original image and such that the evaluation correlates with the human visual system.

Advances in image acquisition technology encouraged increasing interest in the use of magnetic resonance imaging (MRI) system images for the study of human anatomy [5], [6] diagnosis of diseases [7], [8] and the clinical trials of drugs for treatment of neurological diseases [9], [10], [11]. The attractive feature of a MRI system is its potential to produce high contrast images of soft anatomical structures. This potential is an ideal expectation because of imperfections of the system component, trade-offs in system operating parameters, patient induced artifact and operator error. The perceived visual quality of a MRI image of the brain is influenced by features that manifest in the image. The features include noise at different levels, intensity non-uniformity, acquisition artifacts, blurring, geometric distortion, lesion load and extraneous artifacts introduced by image processing and image analysis algorithms. These features influence each other as well as the classical terms of perception such as sharpness, contrast and saturation, and thus makes image quality evaluation a nontrivial task [2].

A. Literature Review

Several objective image quality measures have been proposed in the literature. They can be categorized into reference methods [12], [13], [14], [15], [16] and no-reference methods [17], [18], [19], [20], [21]. Detailed review of image quality evaluation for a general class of images and MRI images can be found in [22], [23], [24], [25],[26], [27], [28], [29]. Despite the several contributions on image quality the popular quality assessment metrics for medical images are the age-old techniques; root-mean-square error (RMSE), signal-to-noise ratio (SNR) and structural similarity index (SSIM) [12]. These metrics were designed to solve research problems that were not related to image interpretation but on efficient compression, storage and transmission of images. We identified six draw-backs in current automated image quality assessment methods. They are explained below:

1) *Generalization of Medical Images*
   The popular quality evaluation metrics assume that all classes of medical images and all other natural images have same descriptive features. Medical images exhibit characteristics such as texture, gray-scale color, noise and homogeneity which distinguish them from each other and other classes of natural images.

2) *Globalization*
   Quality assessments in [12], [13], [19], [20], [21] takes into account the entire image and does not allow focus towards region-of-interest. In some clinical applications such as the study of disease progression in multiple sclerosis the focus is detection of lesions in the white matter region. With global quality measures there is the risk of non-optimal quality measure in a region which is the focus of the physician or a trained reader.

3) *Distortion-Specific Bias*
   Many current quality assessment methods such as [17], [19] adopt specific type of distortion, considered as common, to evaluate the image under consideration. This approach can be said to be biased towards specific distortion because all possible distortions combine with ideal features to manifest as image attribute [18].

4) *Fidelity Bias*
   Image quality as viewed by the human visual system can be represented in three dimensions: fidelity,

usefulness and naturalness. Researchers have argued that the use of reference images such as in [12] for quality evaluation is a measure of fidelity and does not account for the other two attributes of image quality

5) *Limitations of Classical Statistics*

All the current quality assessment metrics adopt the principles of classical statistics to describe quality attributes. Classical statistics does not account for the distinct geographic patterns of the constituent anatomic structures in medical images. The absence of spatial dependency in the description of these attributes excludes the naturalness of the image in the evaluation of image quality. The inability of popular image quality measures to perceptually distinguish different images was reported in [14]. The authors demonstrated that two images with the same root-mean-square error (RMSE) can be perceptually dissimilar. They proposed a technique called null space analysis for quality evaluation.

6) *Complexity Induced by Disease Signatures*

Presence of disease signatures such as lesions in the white matter structures in the brain of multiple sclerosis patients mimic edges of anatomic structures and spurious details. This makes quality measure complicated. The performance of edge-based brain MRI quality measures can be unreliable in the presence of high lesion load.

B. Importance of Automated Objective Quality Measures

There are many real-world applications where there is little room to operate the human visual system method for the evaluation of image quality. A typical scenario is in clinical research organizations. Several thousands of brain MRI images are delivered daily from clinical trial sites around the globe to clinical research organizations that manage clinical trials of new drugs for pharmaceutical organizations. Variations in the quality of images acquired with different scanners from the different clinical trial sites need to be quantified to ensure conformity with protocols set out by sponsoring pharmaceutical organizations. Efficient management of this large amount of data demands high level of automation in the methods of quality assessment of the MRI images. There is little tolerance for subjective quality measures because they are manual, time consuming and lack repeatability. No-reference, objective and automatic quality measures are preferred because they can be computed in real-time and are repeatable. Objective quality measures encourages efficient data management by the classification of images for assignment of real-time automated processing, manual processing and, if necessary, further processing to improve image quality.

C. Introduction to Spatial Statistics

Spatial statistics [30] is a branch of classical statistics. It is a relatively new area in statistics. It became an active research area because of the limitations of classical statistics to solve some real-world problems. There are three major techniques in spatial statistics. They are geostatistics, spatial point patterns and lattice data. For the purpose of this research our interest is in the area of geostatistics. Geostatistical technique focus on fixed spatial region such as a geographical region for the modeling of continuous variables, data prediction from the relationship between variables and evaluation of spatial structures. It can distinguish the visual perception of images by incorporating information about their spatial dependencies. Data from brain images acquired by MRI system have characteristics suitable for spatial analysis. Three dimensional display of brain MRI image reveals clearly defined pattern in the spatial location and the spatial arrangement of the anatomical structures of the brain. The data are continuous variables describing different anatomic structures within a fixed spatial region. The nomenclature adopted for the acquisition planes and some of the constituent anatomic structures: axial, sagittal, coronal, left hemisphere, right hemisphere and mid-sagittal plane are borrowed from the field of geography to describe spatial locations within the brain. The spatial arrangement is the most important attribute of MRI image that is easily perceived by an observer. Every trained reader has the knowledge that the brain is approximately symmetrical with respect to the mid-sagittal plane, the lateral ventricle is approximately centered on the mid-sagittal plane and farther

from the brain surface than the cortical grey matter [31], [32]. After careful review of the literature we can say that, to the best of our knowledge, there is yet no proposal on the application of the principles of spatial statistics to the evaluation of image quality.

D. Our Proposal

We propose a new fully automated, no-reference, objective method to evaluate the quality of MRI system images. It is based on encoding different image quality attributes with local entropy and the similarity in the geometry of human anatomy across age, gender and race [33], [34], [35]. The human brain is regarded to be located in a fixed spatial region which exhibit distinct and organized patterns. The spatial region is regionalized by segmenting each slice in the MRI volume data into eight equal angular segments of 45 degrees. The sample space is the the set which elements are the normalized entropy at each pixel location within a segment in the the foreground of the image. The sample space is partitioned into two regions, low entropy region and high entropy region. The regionalized random variable is the ratio of sum of the normalized entropy within a segment to the total number of pixels within the same segment. Four spatial quality models were built from brain MRI images of 250 subjects sourced from the Alzheimer's disease neuroimaging initiative (ADNI) database. They are area, semivariogram, nugget of semivariogram and the sill of semivariogram. Given a test MRI volume data, quality features corresponding to the four quality models are extracted. Quality score of each feature is computed by comparison to corresponding quality models. Experimental results shows that our proposal correlate with different levels of degradation and for this reason it can be said to correlate with human visual perception.

E. Outline

This paper is organized as follows. The next section explain the theory behind our proposal. Section III describe our methods for evaluation of image quality. Experiment on quality assessment of test images is in section IV. Experimental results are discussed in section V. Section VI concludes this report.

II. THEORETICAL BACKGROUND

The theory section begins with the relationship between the local entropy of an image and the classical quality attributes. The Geostatistics model of brain MRI image is explained, followed by definition of quality models and the law of total probability.

A. Relationship between Local Entropy and Classical Quality Attributes

Entropy is a term borrowed from the field of physics to describe the spread in the energy states of particles within a closed system. It describes the disorderliness of energy states in the system. When adapted to images entropy quantifies the diversity in the composition of pixel intensity levels. The particles are the pixel locations and energy states are the possible intensity levels. In a 8-bit grayscale image there 256 possible intensity levels ranging from 0 to 255 at each pixel location. Local entropy $E(I(x,y))$ is a function of probability $P(I(x,y))$ of a pixel $I(x,y)$ located at the center (x,y) of a $N \times N$ local region B within an image I:

$$E(I(x,y)) = -\sum_x \sum_y P(I(x,y)) \log_2 P(I(x,y)) \tag{1}$$

The probability is directly proportional to the sum of the absolute difference between the intensity level of the center pixel and its $(N^2 - 1)$ immediate neighbors indexed by g;

$$P(I(x,y)) \propto \sum_{g=1}^{N^2-1} \|I(x,y) - B_g\| \tag{2}$$

The expression in Eq. 2 is a measure of the local contrast. The probability of the absolute difference in the horizontal direction:

$$P_y(I(x,y)) \propto \sum_{n_y} \|I(x,y) - \mathbf{B}_{gy}\| \tag{3}$$

and the probability of the absolute difference in the vertical direction:

$$P_x(I(x,y)) \propto \sum_{n_x} \|I(x,y) - \mathbf{B}_{gx}\| \tag{4}$$

is a measure of sharpness which is the amount of details and contrast along edges in the local region

Equation 2 can be simplified by computing the mean brightness of the local region so that $P(I(x,y))$ is expressed as deviation from the mean μ_B, the luminous brightness of the local region

$$P(I(x,y)) \propto \|I(x,y) - \mu_{\mathbf{B}}\| \tag{5}$$

and as a function of the variance σ_B^2, a measure of noise level in the local region

$$P(I(x,y)) \propto \|I(x,y) - \mu_{\mathbf{B}}\|^2 = \sigma_B^2 \tag{6}$$

Thus entropy is a direct measure of the classical image quality attributes; luminous brightness, contrast, sharpness, noise and texture.

B. Geostatistical Model of Brain MRI image

The geostatistic model of brain MRI image is built from W ideal quality MRI volume data. Each data consist of K useful slices so that the total number of slices in the database is $Z = KW$ where $Z = \{z|1, \cdots, Z\}$.

1) Geographic Region: The geographic region $\mathbf{s}$ is an hypothetical 3D cylindrical coordinate system of unit radius and height T shown in Fig. 1:

$$\mathbf{s} = \{r, \theta, t | 0 \leq r \leq 1, -\pi \leq \theta \leq \pi, 1 \leq t \leq T\} \in \mathbf{R^3} \tag{7}$$

where r and θ are the radial and angular distances of pixel locations in the foreground of each slice. The geographic region is regionalized as shown in Fig. 2 by patching the foreground of each slice into Q equal angular segments

$$\theta_q = \left\{ \left(-\pi + (q-1)\frac{2\pi}{Q} \right) < \theta < \left(\pi + (q-Q)\left(\frac{2\pi}{Q}\right) \right) \right\} \tag{8}$$

where $q = \{1, 2, ..., Q\}$.

2) Sample Space: The sample space S consist of the distribution of normalized local entropy λ within each angular segment $q(r, \theta, z)$ in a slice $z \in Z$:

$$S = \{\lambda_{q(r,\theta,z)} : 1 \leq q \leq Q, 0 \leq \lambda \leq 1\} \tag{9}$$

For some global threshold τ we partition the sample space into low entropy region S_L:

$$S_L = \{\lambda_{q(r,\theta,z)} : 1 \leq q \leq Q, 0 \leq \lambda \leq \tau\} \tag{10}$$

and high entropy region S_H:

$$S_H = \{\lambda_{q(r,\theta,z)} : 1 \leq q \leq Q, \tau < \lambda \leq 1\} \tag{11}$$

such that:

$$S = S_L \cup S_H \tag{12}$$

3) Random Variable: In the model database there are $Z \times Q$ feature vectors indexed by $\{q|1, \cdots, Q\}$ angular segments. If Z is large enough such that $Z \gg Q$, then Z feature vectors generated from the database will be randomly distributed into each angular segment in the hypothetical cylindrical coordinate system of Fig. 1. A random variable X is defined as a function that assigns a real number $X(\lambda)$ to each outcome λ in the sample space S of a random experiment [36]. We express the random variable as the ratio of the sum of normalized local entropy values $\lambda_{q(r,\theta,z)}$ within an angular segment of a slice z to the total number of pixels n_q within the angular segment.

$$X_q(\lambda) = \frac{\sum \lambda_{q(r,\theta,z)}}{n_q} \qquad (13)$$

The random variable is expressed to reflect the partitioning of the sample space into low and high entropy regions;

$$X_{qL} = \{x_{qL1}, x_{qL2}, \cdots, x_{qLZ}\} \qquad (14)$$

$$X_{qH} = \{x_{qH1}, x_{qH2}, \cdots, x_{qHZ}\} \qquad (15)$$

4) Regionalized Variable: The random variables expressed in Eq. 13, Eq. 14 and Eq. 15 are distributed over space **s**, and thus can be regarded as regionalized variable $X(s)$:

$$\{X(\mathbf{s}) : \mathbf{s} \in \mathbf{R}^3\} \qquad (16)$$

where $\mathbf{s} = s(r, \theta, t)$. Regionalized variable like the classical random variable exhibit random characteristic at a specific location **s**. However, unlike the classical random variable they possess structured spatial characteristics because they are distributed over space [37].

5) Semivariogram: The semivariogram is a function that measures the rate of change of a regionalized variable with distance [38]. Given that $X(\mathbf{s})$ and $X(\mathbf{s+t})$ are measurements of a regionalized variable at K finite locations separated by distance t, the semivariogram V is expressed as.

$$V(t) = \frac{1}{2K} \sum_{i=1}^{K} [X(\mathbf{s}_i) + X(\mathbf{s}_i + t_i)]^2 \qquad (17)$$

Semivariogram is a description of the squared difference between successive points in a region of interest and assigns spatial correlation structure to the data. An example of the plot of a theoretical semivariogram is shown in Fig. 3 [39]. There are three notable features in the profile. The nonzero intercept of the variogram called the nugget effect gives an estimate of measurement error and variability within the spatial region. The sill corresponds to the maximum height of the variogram and gives an estimate of the variance of the region of interest. The range of influence is the distance beyond which successive locations have negligible spatial correlation.

The definition of the semivariogram in Eq. 17 requires the regionalized variable to vary across slices hence the semivariogram is applicable only to multi-slice MRI volume data and not to a single slice. Given that the semivariogram is quantized into P linearly spaced points, there will be $L = P \times Q$ semivariogram feature vectors for each MRI volume data and $W \times L$ feature vectors for the entire database.

$$V = \begin{pmatrix} v_{w1,l1}, v_{w1,l2}, \ldots, v_{w1,L} \\ v_{w2,l1}, v_{w2,l2}, \ldots, v_{w2,L} \\ \ldots\ldots\ldots\ldots\ldots \\ \ldots\ldots\ldots\ldots\ldots \\ v_{W,l1}, v_{W,l2}, \ldots, v_{W,L} \end{pmatrix} \qquad (18)$$

C. Quality Models

The random variables X_{qL} and X_{qH} expressed in Eq. 14 and Eq. 15, respectively are defined within a finite interval, $\{0 \leq x \leq 1\}$. For each volume data their mean and variance are finite:

$$\mu_{x_{wL}} = \frac{1}{K} \sum_{k=1}^{k=K} x_{kL} \tag{19}$$

$$\mu_{x_{wH}} = \frac{1}{K} \sum_{k=1}^{k=K} x_{kH} \tag{20}$$

$$\sigma^2_{x_{wL}} = \frac{1}{K} \sum_{k=1}^{k=K} (x_{kL} - \mu_{x_{wL}})^2 \tag{21}$$

$$\sigma^2_{x_{wH}} = \frac{1}{K} \sum_{k=1}^{k=K} (x_{kH} - \mu_{x_{wH}})^2 \tag{22}$$

The central limit theorem states that the distribution will tend to a Gaussian [40],[36],[41]. We now define two quality models, the low entropy area X_{A_L} quality model:

$$P(X_{A_L}) = \frac{1}{\sqrt{2\pi}\sigma_{X_{A_L}}} \exp - \left(\frac{(X_{A_L} - \mu_{A_L})^2}{2\sigma^2_{X_{A_L}}} \right) \tag{23}$$

and the high entropy area X_{A_H} quality model:

$$P(X_{A_H}) = \frac{1}{\sqrt{2\pi}\sigma_{X_{A_H}}} \exp - \left(\frac{(X_{A_H} - \mu_{A_H})^2}{2\sigma^2_{X_{A_H}}} \right) \tag{24}$$

The third quality model is the variogram quality model, a $1 \times L$ matrix derived from the mean, along the column dimension of the semivariogram expressed in Eq. 18:

$$V_r = \frac{1}{W} \sum_{w=1}^{w=W} \sum_{l=1}^{l=L} V_{w,l} \tag{25}$$

The expression in Eq. 25 can be resized into a $P \times Q$ matrix;

$$V_{rr} = \begin{pmatrix} v_{p1,q1}, v_{p1,q2}, \ldots, v_{p1,Q} \\ v_{p2,q1}, v_{p2,q2}, \ldots, v_{p2,Q} \\ \ldots\ldots\ldots\ldots\ldots\ldots \\ \ldots\ldots\ldots\ldots\ldots\ldots \\ v_{P,q1}, v_{P,q2}, \ldots, v_{P,Q} \end{pmatrix} \tag{26}$$

where each column is the mean semivariogram of each angular segment. The first element in each column is the nugget and the last element is the sill. We define the first row of the resized matrix as the fourth quality model and is referred to as the nugget of the semivariogram:

$$V_{ng} = \{v_{p1,q1}, v_{p1,q2}, \ldots, v_{p1,Q}\} \tag{27}$$

The fifth quality model is the absolute difference between the nugget and the sill in each angular segment. This model is referred to as the sill quality model

$$V_{sl} = \{\|v_{p1,q1} - v_{P,q1}\|, \|v_{p1,q2} - v_{P,q2}\|, \ldots, \|v_{p1,Q} - v_{P,Q}\|\} \tag{28}$$

D. *The Law of Total Probability*

We denote the feature vector extracted from a test image as α. The extent to which the area feature vector $\alpha_{A_L}, \alpha_{A_H}$ extracted from a test image normalizes the area quality model in Eq. 23 and Eq. 24 is the area feature quality score $\gamma_{A_L}, \gamma_{A_H}$ for the test image:

$$\gamma_{A_L} = \frac{1}{\sqrt{2\pi}\sigma_{X_{A_L}}} \exp - \left(\frac{(\alpha_{A_L} - \mu_{A_L})^2}{2\sigma_{X_{A_L}}^2} \right) \tag{29}$$

$$\gamma_{A_H} = \frac{1}{\sqrt{2\pi}\sigma_{X_{A_H}}} \exp - \left(\frac{(\alpha_{A_H} - \mu_{A_H})^2}{2\sigma_{X_{A_H}}^2} \right) \tag{30}$$

For any given feature vector of a test image including the area feature vectors α_{A_L}, α_{A_H}, the law of total probability is applied to compute the quality scores because the sample space is partitioned by the low and the high entropy regions. Given the variogram feature vector α_{V_r} the variogram quality score γ_{V_r} is:

$$\gamma_{V_r} = P(\alpha_{V_r})P(\alpha_{V_r}|\alpha_{A_L}) + (1 - P(\alpha_{V_r}))P(\alpha_{V_r}|\alpha_{A_H}) \tag{31}$$

where

$$P(\alpha_{V_r}) = \|V_r - \alpha_{V_r}\| \tag{32}$$

$$P(\alpha_{V_r}|\alpha_{A_L}) = \gamma_{A_L} \tag{33}$$

$$P(\alpha_{V_r}|\alpha_{A_H}) = \gamma_{A_H} \tag{34}$$

Given the nugget feature vector $\alpha_{V_{ng}}$ the nugget quality score $\gamma_{V_{ng}}$ is:

$$\gamma_{V_{ng}} = P(\alpha_{V_{ng}})P(\alpha_{V_{ng}}|\alpha_{A_L}) + (1 - P(\alpha_{V_{ng}}))P(\alpha_{V_{ng}}|\alpha_{A_H}) \tag{35}$$

where

$$P(\alpha_{V_{ng}}) = \|V_{ng} - \alpha_{V_{ng}}\| \tag{36}$$

$$P(\alpha_{V_{ng}}|\alpha_{A_L}) = \gamma_{A_L} \tag{37}$$

$$P(\alpha_{V_{ng}}|\alpha_{A_H}) = \gamma_{A_H} \tag{38}$$

Given the sill feature vector $\alpha_{V_{sl}}$ the sill quality score $\gamma_{V_{sl}}$ is:

$$\gamma_{V_{sl}} = P(\alpha_{V_{sl}})P(\alpha_{V_{sl}}|\alpha_{A_L}) + (1 - P(\alpha_{Vsl}))P(\alpha_{V_{sl}}|\alpha_{A_H}) \tag{39}$$

where

$$P(\alpha_{V_{sl}}) = \|V_{sl} - \alpha_{V_{sl}}\| \tag{40}$$

$$P(\alpha_{V_{sl}}|\alpha_{A_L}) = \gamma_{A_L} \tag{41}$$

$$P(\alpha_{V_{sl}}|\alpha_{A_H}) = \gamma_{A_H} \tag{42}$$

III. METHODS

This section begins with the setup of the experiment. It explains the choice of a suitable data for the model database. This is followed by modeling experiment which explains how the database feature vectors were generated. The section ends with the derivation of quality models from the feature vectors. The algorithm was implemented in the MatLab computing environment. The flow chart in Fig. 4 introduce our methods. Model image **MIM** are the elements of the modeling experiment **MEX** for generating model feature database **FED**. Quality models **QM** are computed from the feature database using probability density function **PDF** technique. Given a test image **TIM** features are extracted **FEX** to create feature vectors **FV**. Quality features **QF** are determined from classification **CL**. Quality measure **QM** compare the quality features **QF** of the test image with the corresponding quality model **QM** of the model images to determine the quality score **QS**.

A. Setup of Modeling Experiment

T1-weighted MRI images acquired using three-dimensional magnetization-prepared rapid gradient echo (MPRAGE) technique was our choice for the model database images. Images acquired using MPRAGE pulse sequence exhibit superior gray-white matter contrast compared to the conventional T1 and other structural brain MRI images [42], [43], [44]. Two hundred and fifty high quality, high resolution, 3D, T1-weighted MPRAGE MRI images were sourced from the Alzheimer's disease neuroimaging initiative (ADNI) database (www.adni.loni.usc.edu). Each slice has thickness of 1.2 mm and dimension of 190×160. The pixel intensity levels are stored as unsigned 16-bit integers. Details of ADNI acquisition protocol and the initial processing steps are available in [45]. During data sourcing at ADNI website we seek MRI data of patients with healthy and normal brains that were without lesions or with very mild lesions. For each MRI data, slices towards the most inferior and most superior sections are discarded because they highlight more of scalp and bone structures than brain structures. There are variations in the number of useful slices for different patients. For each patient data the index of useful slices were coded in a special function which can be called up by the algorithm during the modeling experiment.

B. Modeling Experiment

Graphical description of the modeling experiment can be explained using the flow chart in Fig. 5.

1) Foreground Extraction: Foreground function **FR** extracts foreground **FI** from each slice in a volume data. The centroid and the number of elements in each foreground are recorded.

2) Local Entropy Filtering: Local entropy image **LEI** of each slice is computed using local entropy filter **ENF** of size 3×3.

3) Binary Transformation: The mean of the local entropy image is determined and used as a global threshold for transformation **BT** to the binary domain. Pixel locations in the binary image **BEI** is transformed from the classical cartesian coordinate system to cylindrical coordinate system. In the cylindrical coordinate system the binary image is partitioned into eight equal angular segments of 45 degrees.

4) Local Entropy Classification: The global threshold for binary transformation is used as criteria for classifying **CL** the local entropy image into low **LOW** and high **HIGH** entropy regions.

5) Feature Extraction (FEX): The number of pixels in each of the low and high entropy regions are determined. The number of pixels in each region is divided by the number of pixels in the foreground to determine the pixel density for each region. The pixels density for each region in all the slices in a volume data are summed and averaged to obtain a single pixel density for a volume data. The pixel density feature vector for the model database is a 1×250 random variable for each of the low and high entropy regions.

Angular pixel density is the ratio of sum of entropy values in each angular segment to the total number of pixels in the same angular segment. Eight angular pixel density are computed for each slice. Each angular pixel density is an element of a $1 \times K$ column vector where K is the number of slices in a volume data. The semivariogram of the feature vector is computed for each angular segment. There are variations in the number of useful slices for each patient. To ensure uniformity in the size of the feature vectors for all the data in the database the semivariogram is quantized into 10 linearly spaced column vector. Thus there are a total of 10×8 semivariogram feature vector for each volume data. Each column is normalized to lie between 0 and 1. Thereafter the feature vector is resized to a 1×80 feature vector. For the entire database we obtain a 250×80 semivariogram feature vector.

C. Quality Models

Five quality models were generated from the modeling experiment. Two of the models are Gaussian distributions derived from the random variables representing the low and high entropy regions. The random variables were modeled as Gaussian distributions because the process of their generation conform with the central limit theorem. The distributions were centered at the mean of the random variables. The standard

deviation was set such that 47.5 percent of all the random variables lie between 0 and its mean so that 95 percent of all the random variables will lie on either side of the mean for a normally distributed Gaussian distribution.

Three quality models were derived from the semivariogram. They are the normalized variogram, the nugget and the sill. The normalized variogram is the mean of the semivariogram feature vector along the column dimension, a 1×80 quality model. The nugget and the sill are derived from the normalized variagram, resized to a 10×8 quality model. The first row of the resized data, a 1×8 vector representing the minimum values of the semvariogram in each angular segment is the nugget quality model. Absolute value of difference between the first and last row of the resized variogram is the sill quality model.

IV. Experimental Results

A. Setup of Experiment

Performance evaluation of our proposal was carried out using original MRI data from two different sources. They are NeuroRx research Inc and BrainCare Oy. NeuroRx inc. (https://www.neurorx.com) is a clinical research organization dedicated to working with the pharmaceutical industry to facilitate clinical trials of new drugs for multiple sclerosis (MS) and other neurological diseases. BrainCare Oy (http://braincare.fi/) is a Tampere University of Technology spin-off company founded in 2013 to deliver personalized solutions to improve the quality of life of epilepsy patients. The organization recently concluded clinical trials for a novel mobile application and supporting solutions for long-term monitoring for epileptic patients.

There are two original T1-weighted and one original FLAIR images from NeuroRx research Inc. All the data from NeuroRx has same slice thickness of 2.4 mm, dimension 256×256 and consist of 60 slices. The image quality were considered within acceptable limits. Slices of the T2-weighted data from NeuroRx are displayed in Fig. 6 and Fig. 9. A slice from the FLAIR data is shown in Fig. 8. The data from BrainCare Oy are one original T2-weighted data with high lesion load and dimension 240×200 and another original T2-weighted image with dimension 480×360. They have same slice thickness of 7.5mm and consists of 25 slices. Both data from BrainCare are considered good quality. Slices from the T2-weighted data can be viewed in Fig. 7 and Fig. 12.

Quality evaluation was carried out on the test images in their original state and in their noisy and blurred versions. The different levels of noise and blur range from 0 to 10.

B. Quality Assessment Experiment

The initial steps in the quality assessment of a test image is depicted in Fig. 6. A slice of the test image is in Fig. 6a. The image is rotated by 180 degrees as shown in Fig. 6b so as to be in the same orientation as the model images. Foreground extracted from the rotated image is shown in Fig. 6c. Local entropy of the test image computed using a 3×3 local entropy filter is shown in Fig. 6d. Figure 6e and Fig. 6f show the low and the high entropy regions that were extracted by transforming the local entropy image into a binary image. The area density or ratio of the number of pixels in both regions to the number of pixels in the foreground are computed. The area density for the low and high entropy regions for all the slices in the volume data are summed and averaged. Pixel locations of the extracted entropy regions are transformed to the cylindrical coordinate system. Each of the two region images are patched into 8 angular segments of 45 degrees. Feature density in each angular segment, for all the slices, are computed to form a column vector with length equal to the number of slices in the volume data. The semivariogram of the data is computed, mormalized to lie between 0 and 1 and quantized to 10 linearly spaced data points. The normalized semivariogram of the MRI volume data is a 10×8 feature vector which is resized to a 1×80 data. The nugget feature vector is the first row of the 10×8 normalized semivariogram feature vector. The sill feature vector is the absolute difference between the first and last rows of the semivariogram.

The area quality scores for the low and high entropy regions are determined according to Eq. 29 and Eq. 30, respectively. The semivariogram quality score, the nugget quality score and the sill quality score are computed according to Eq. 31, Eq. 35 and Eq. 39 respectively.

1) MRI Volume Data: Results of quality evaluation of T2-weighted MRI volume data from BrainCare is displayed in Fig. 7. Presence of lesions in the white matter region is obvious in the slice shown in Fi.g 7a. Plot of the low entropy and high entropy area quality scores are displayed in Fig. 7b. Variogram quality scores in each angular segment of the volume data are displayed in Fig. 7c. For each angular segment the quality score for the low and high entropy regions are displayed. The sill quality score for the low and high entropy regions in each angular segment is displayed in Fig. 7d

Figure 8a is a slice in a FLAIR volume data from NeuroRx. The area quality scores for the low and high entropy regions are shown in Fig. 8b. The variogram quality score is in Fig. 8c and the sill quality score is in Fig. 8d.

2) Blur Degradation: Images in Fig. 9 explains different levels of degradation in a T2-weighted MRI volume data from NeuroRx. The image in Fig. 9a is one of the 60 slices in a MRI volume data. The image in Fig. 9b is degraded by insignificant level of blur, blur level=1. The blur level is significantly increased to 5 as shown in Fig. 9c. Figure 9d shows very severe degradation of the original image, blur level=10.

The bar plots in Fig. 10a, Fig. 10b and Fig. 10c are the semivariogram plots of the low and high entropy regions for the third angular segment of the volume data for blur level=1, blur level=5 and blur level=10, respectively. Figure 10d shows the variation of the semivariogram (high entropy region) for successive different levels of blur ranging from 0 to 10. Variations of the four quality scores, the area, the variogram, (low entropy region) the nugget and the sill for different levels of blur are displayed in Fig. 11a, Fig. 11b, Fig. 11c and Fig. 11d, respectively.

3) Noise Degradation: Figure 12 shows a slice in a T2-weighted MRI volume data from BrainCare. The slice in Fig. 12a is the original slice. Different levels of Rician noise degradation of the original image, 1 percent, 5 percent and 10 percent are displayed in Fig. 12b, Fig. 12c and Fig. 12d, respectively.

Semivariograms corresponding to Rician noise levels of 1 percent, 5 percent and 10 percent are displayed in Fig. 13a, Fig. 13b and Fig. 13c, respectively. Variation of semvariogram (high entropy region) for increasing levels of Rician noise is shown in Fig. 13d. The area quality score, the variogram (high entropy region) quality score, nugget quality score and the sill quality score for different levels of Rician noise are displayed in Fig. 14a, Fig. 14b, Fig. 14c and Fig. 14d, respectively.

V. Discussion

A. Correlation with Acceptable Quality Images

The plots in Fig. 7 and Fig. 8 demonstrate that our proposal can accurately assess good quality MRI volume data. The area quality score of T2-weighted data for the low entropy region denoted by the index 1 is close to the ideal as shown in Fig. 7b. The area quality score for the high entropy region is about 0.85. Quality scores of each element of the 1×10 semivariogram shown in Fig. 7c for the third angular segment conforms with the level of image quality. The sill quality score in Fig. 7d for each of the 8 angular segment conform with the quality of data. It varies from 0.5 to 0.9.

The area quality scores for both the low and high entropy regions of slices in the FLAIR volume data (a slice is shown in Fig. 8a) are close to 0.9 as shown in Fig. 8b. In Fig. 8c the average quality score of each semivariogram element for the third angular segment is about 0.9. The sill quality score in Fig. 8d for each angular segment has average of 0.7 which is a reflection of the good quality status of the volume data.

B. Correlation with Variations in Image Quality

Our proposal can objectively differentiate images having different levels of image quality. The bar plots in Fig. 10a, Fig. 10b and Fig. 10c correlate with the three different levels of blur degradation. In Fig. 10d variations of the semivariogram correlate with successive blur degradation, from 1 to 10. The area quality score in Fig. 11a, the variogram quality score in Fig. 11b, the nugget quality score in Fig. 11c and the sill quality score in Fig. 11d also correlate with different levels of blur degradation.

The bar plot in Fig. 13a, Fig. 13b and Fig. 13c correlate with Rician noise levels of 1 percent, 5 percent and ten percent, respectively. In Fig. 13d the semivsriogram correlate with successive Rician noise levels, from 1 to 10 percent. The area quality score, the variogram quality score, the nugget quality score and the sill quality score in Fig. 14a, Fig. 14b, Fig. 14c and Fig. 14d also demonstrates how our proposal correlate with different levels of Rician noise.

C. Focus towards Region-of-Interest

Our proposal assess image quality at two spatial resolutions. In the first spatial resolution the image is classified into low and high entropy regions. Quality assessment in the low and high entropy regions enables focus towards the white matter and gray matter regions, respectively. The second spatial resolution encourages finer focus towards region of interest as the volume data is patched into eight equal angular segments.

D. Robustness to Presence of Lesions

In T1-weighted images lesions in the white matter region are hypointense. The hypointense lesions mimic gray matter regions. The edges of the lesions also mimic spurious edges which can result from the presence of noise. In MRI volume data with high lesion load this features can 'fool' automated objective quality assessment algorithms to give erroneous results. Our proposal is robust to high lesion load by partitioning each slice into low and high entropy regions and applying the law of total probability.

E. Robustness to Spatial Dependency

The design of our proposal takes into account the spatial relationship between the constituent anatomic structures of the brain. The variogram quality score quantifies image quality using inter-slice information and the area quality score quantifies image quality using intra-slice information in the volume data.

F. Correlation with the Human Visual System

When any of the blur and noise distortion increases the visual quality of the image is decreased as shown in Fig. 10, Fig. 11, Fig. 13 and Fig. 14, and because of this our proposal can be said to correlate with the human visual system in terms of usefulness, fidelity and naturalness. The usefulness is derived from the use of brain MRI data from subjects across age, gender and age to build quality models. The fidelity comes from comparing a test data with the quality models. The naturalness is derived by the application of semivariogram to quantify spatial correlation between constituent anatomic structures.

VI. Conclusion

In this report we propose a new method to evaluate the quality of brain MRI images. It is based on the principle of geometric similarity of human anatomy acorss age, gender and race. The principle of spatial statistics is applied on database of brain MRI images to generate quality models. An MRI image is evaluated based on how its extracted feature compares with corresponding quality model. Our proposal incorporates directional information and spatial dependencies of anatomic structures and this encourages image quality evaluation based on region-of-interest.

References

[1] M. Pedersen, Y. Zheng, and J. Hardeberg, "Evaluation of image quality metrics for color prints," in *Image Analysis*, ser. Lecture Notes in Computer Science, A. Heyden and F. Kahl, Eds. Springer Berlin Heidelberg, 2011, vol. 6688, pp. 317–326.

[2] M. Pedersen, N. Bonnier, J. Y. Hardeberg, and F. Albregtsen, "Attributes of image quality for color prints," *Journal of Electronic Imaging*, vol. 19, no. 1, pp. 011 016–011 016–13, 2010.

[3] Z. Wang and A. Bovik, *Modern Image Quality Assessment*. Morgan & Claypool, 2006.

[4] R. Janssen, *Computational Image Quality*, ser. Press Monographs. Society of Photo Optical, 2001.

[5] H. M. Duvernoy, *The human brain: surface, three-dimensional sectional anatomy with MRI, and blood supply*. Springer Science & Business Media, 2012.

[6] S. Mori, S. Wakana, P. C. Van Zijl, and L. Nagae-Poetscher, *MRI atlas of human white matter*. Am Soc Neuroradiology, 2005, vol. 16.

[7] G. B. Frisoni, N. C. Fox, C. R. Jack, P. Scheltens, and P. M. Thompson, "The clinical use of structural mri in alzheimer disease," *Nature Reviews Neurology*, vol. 6, no. 2, pp. 67–77, 2010.

[8] P. Scheltens, D. Leys, F. Barkhof, D. Huglo, H. Weinstein, P. Vermersch, M. Kuiper, M. Steinling, E. C. Wolters, and J. Valk, "Atrophy of medial temporal lobes on mri in" probable" alzheimer's disease and normal ageing: diagnostic value and neuropsychological correlates." *Journal of Neurology, Neurosurgery & Psychiatry*, vol. 55, no. 10, pp. 967–972, 1992.

[9] D. L. Arnold, P. A. Calabresi, B. C. Kieseier, S. I. Sheikh, A. Deykin, Y. Zhu, S. Liu, X. You, B. Sperling, and S. Hung, "Effect of peginterferon beta-1a on mri measures and achieving no evidence of disease activity: results from a randomized controlled trial in relapsing-remitting multiple sclerosis," *BMC neurology*, vol. 14, no. 1, p. 1, 2014.

[10] K. Selmaj, L. Kappos, D. Arnold, E. Havrdova, A. Boyko, M. Kaufman, H. Wiendl, J. Rose, S. Greenberg, K. Riester *et al.*, "Safety and tolerability results from the decide study: A phase 3 active-comparator study of daclizumab hyp in relapsing-remitting multiple sclerosis (p7. 230)," *Neurology*, vol. 84, no. 14 Supplement, pp. P7–230, 2015.

[11] G. Comi, J. Cohen, D. Arnold, A. Bar-Or, S. Gujrathi, J. Hartung, A. Olson, M. Cravets, P. Frohna, and K. Selmaj, "Efficacy results of the phase 2 portion of the radiance trial: A randomized, double-blind, placebo-controlled trial of oral rpc1063 in adults with relapsing multiple sclerosis (p7. 198)," *Neurology*, vol. 84, no. 14 Supplement, pp. P7–198, 2015.

[12] Z. Wang, A. C. Bovik, H. R. Sheikh, and E. P. Simoncelli, "Image quality assessment: From error visibility to structural similarity," *IEEE Transactions on Image Processing*, vol. 13, no. 4, pp. 600–612, 2004.

[13] M. Narwaria and W. Lin, "Objective image quality assessment based on support vector regression," *IEEE Transactions on Neural Networks*, vol. 21, no. 3, pp. 515–519, March 2010.

[14] F. Prieto, M. Guarini, C. Tejos, and P. Irarrazaval, "Metrics for quantifying the quality of mr images," in *Proceedings of the 17th Annual Meeting of ISMRM*, 2009, p. 4696.

[15] J. Miao, F. Huang, S. Narayan, and D. L. Wilson, "A new perceptual difference model for diagnostically relevant quantitative image quality evaluation: A preliminary study," *Magnetic resonance imaging*, vol. 31, no. 4, pp. 596–603, 2013.

[16] J. Miao, D. Huo, and D. L. Wilson, "Quantitative image quality evaluation of mr images using perceptual difference models," *Medical physics*, vol. 35, no. 6, pp. 2541–2553, 2008.

[17] J. Woodard and M. Carley-Spencer, "No-reference image quality metrics for structural mri," *Neuroinformatics*, vol. 4, no. 3, pp. 243–262, 2006.

[18] A. Mittal, A. Moorthy, and A. Bovik, "No-reference image quality assessment in the spatial domain," *IEEE Transactions on Image Processing*, vol. 21, no. 12, pp. 4695–4708, Dec 2012.

[19] Y. Fang, K. Ma, Z. Wang, W. Lin, Z. Fang, and G. Zhai, "No-reference quality assessment of contrast-distorted images based on natural scene statistics," *IEEE Signal Processing Letters*, vol. 22, no. 7, pp. 838–842, July 2015.

[20] B. Mortamet, M. A. Bernstein, C. R. Jack, J. L. Gunter, C. Ward, P. J. Britson, R. Meuli, J.-P. Thiran, and G. Krueger, "Automatic quality assessment in structural brain magnetic resonance imaging," *Magnetic Resonance in Medicine*, vol. 62, no. 2, pp. 365–372, 2009.

[21] M. Saad, A. Bovik, and C. Charrier, "Blind image quality assessment: A natural scene statistics approach in the dct domain," *IEEE Transactions on Image Processing*, vol. 21, no. 8, pp. 3339–3352 month=Aug,, 2012.

[22] N. Sinha and A. Ramakrishnan, "Quality assessment in magnetic resonance images," *Critical Reviews in Biomedical Engineering*, vol. 38, no. 2, 2010.

[23] M. Pedersen and J. Y. Hardeberg, "Full-reference image quality metrics: Classification and evaluation," *Foundations and Trends in Computer Graphics and Vision*, vol. 7, no. 1, pp. 1–80, 2012.

[24] M. Pedersen, "Evaluation of 60 full-reference image quality metrics on the CID: IQ," in *2015 IEEE International Conference on Image Processing, ICIP 2015, Quebec City, QC, Canada, September 27-30, 2015*, 2015, pp. 1588–1592.

[25] C. Cavaro-Menard, L. Zhang, and P. Le Callet, "Diagnostic quality assessment of medical images: Challenges and trends," in *2010 2nd European Workshop on Visual Information Processing (EUVIP)*, July 2010, pp. 277–284.

[26] K.-H. Thung and P. Raveendran, "A survey of image quality measures," in *2009 International Conference for Technical Postgraduates (TECHPOS)*, Dec 2009, pp. 1–4.

[27] L. Moraru, S. S. Moldovanu, and C. D. Obreja, "A survey over image quality analysis techniques for brain mr images," *International Journal of Radiology*, vol. 2, no. 1, pp. 24–28, 2015.

[28] D. M. Chandler, "Seven challenges in image quality assessment: past, present, and future research," *ISRN Signal Processing*, vol. 2013, 2013.

[29] Z. Wang, "Objective image quality assessment: Facing the real-world challenges," in *Society for Imaging Science and Technology, International Symposium on Electronic Imaging, Image Quality and System Performance XII*, 2016, pp. 1–6.

[30] N. Cressie, *Statistics for spatial data*. John Wiley & Sons, 2015.

[31] O. Colliot, O. Camara, R. Dewynter, and I. Bloch, "Description of brain internal structures by means of spatial relations for mr image segmentation," in *Medical Imaging 2004*. International Society for Optics and Photonics, 2004, pp. 444–455.

[32] D. M. Bowden and R. F. Martin, "Neuronames brain hierarchy," *Neuroimage*, vol. 2, no. 1, pp. 63–83, 1995.

[33] K. Wendel, M. Osadebey, and J. Malmivuo, "Incorporating craniofacial anthropometry into realistically-shaped head models," in *World Congress on Medical Physics and Biomedical Engineering, September 7 - 12, 2009, Munich, Germany*, ser. IFMBE Proceedings, O. Dssel and W. Schlegel, Eds. Springer Berlin Heidelberg, 2010, vol. 25/4, pp. 1706–1709.

[34] M. Osadebey, "Simulation of realistic head geometry using radial vector representation of magnetic resonance image data," Master's thesis, Tampereen teknillinen yliopisto. Julkaisu-Tampere University of Technology., 2009.

[35] K. E. Wendel, "The influence of tissue conductivity and head geometry on eeg measurement sensitivity distributions," Ph.D. dissertation, Tampereen teknillinen yliopisto. Julkaisu-Tampere University of Technology., 2010.

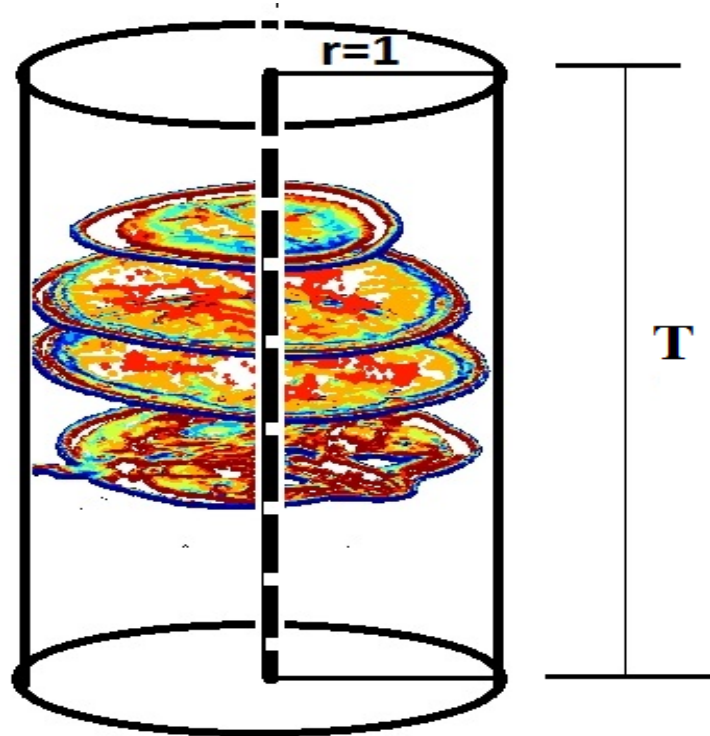MRI VOLUME TRANSFORMED TO CYLINDRICAL COORDINATE STSTEM

Fig. 1. Each MRI slice in a MRI volume is transformed from the original cartesian coordinate system to cylinder coordinate system of unit radius $r = 1$ and height T.

[36] A. Leon-Garcia, *Probability, Statistics and Random Processes for Electrical Engineering*. 3rd edition, Chapter 3: Pearson Education Inc., Prentice Hall, 2008.
[37] G. Matheron, *Principles of geostatistics*. Society of Economic Geologists, 1963, vol. 58, no. 8.
[38] R. A. Olea, *Fundamentals of semivariogram estimation, modeling, and usage*. AAPG Special Volumes, 1994.
[39] A. Biswas and B. C. Si, "Model averaging for semivariogram model parameters," *Advances in Agrophysical Research*, vol. 5, pp. 81–96, 2013.
[40] D. L. Ruderman, "The statistics of natural images," *Network: computation in neural systems*, vol. 5, no. 4, pp. 517–548, 1994.
[41] G. Norman and D. Streiner, *Biostatistics: The Bare Essentials*. 3rd edtion, Chapter 4: People's Medical Publishing House.
[42] N. Shiee, P.-L. Bazin, J. L. Cuzzocreo, C. Ye, B. Kishore, A. Carass, P. A. Calabresi, D. S. Reich, J. L. Prince, and D. L. Pham, "Reconstruction of the human cerebral cortex robust to white matter lesions: method and validation," *Human brain mapping*, vol. 35, no. 7, pp. 3385–3401, 2014.
[43] J. P. Mugler and J. R. Brookeman, "Three-dimensional magnetization-prepared rapid gradient-echo imaging (3d mp rage)," *Magnetic Resonance in Medicine*, vol. 15, no. 1, pp. 152–157, 1990.
[44] P. Reimer, J. F. Meaney, P. M. Parizel, and F. A. Stichnoth, *Clinical MR imaging*. Springer, 2010.
[45] C. R. Jack, M. A. Bernstein, N. C. Fox, P. Thompson, G. Alexander, D. Harvey, B. Borowski, P. J. Britson, J. L Whitwell, C. Ward *et al.*, "The alzheimer's disease neuroimaging initiative (adni): Mri methods," *Journal of Magnetic Resonance Imaging*, vol. 27, no. 4, pp. 685–691, 2008.

AN MRI SLICE DIVIDED INTO ANGULAR SEGEMENTS
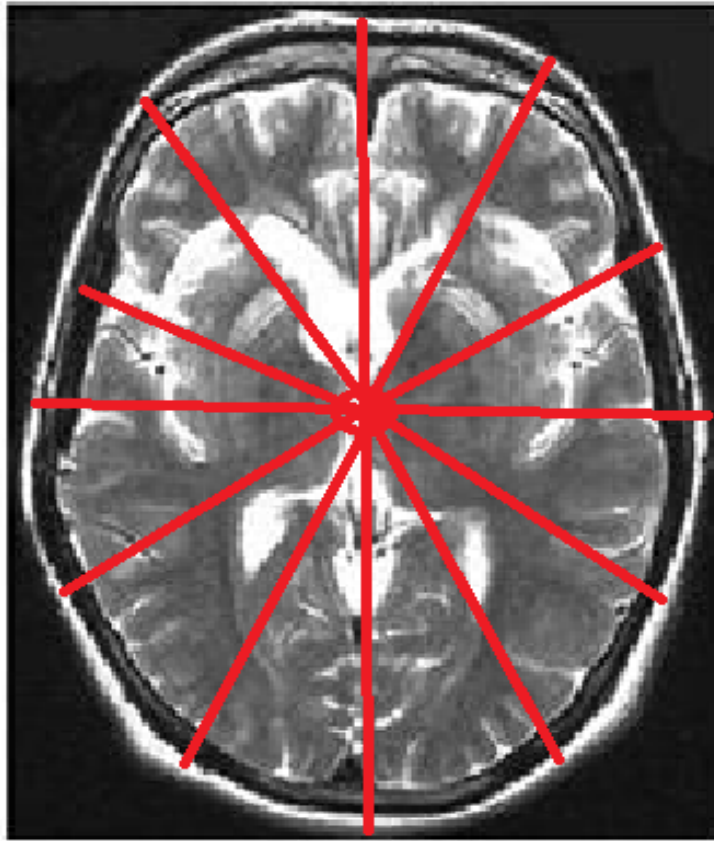
Angular Segments

Fig. 2. The red lines demarcate an MRI slice into angular segments.
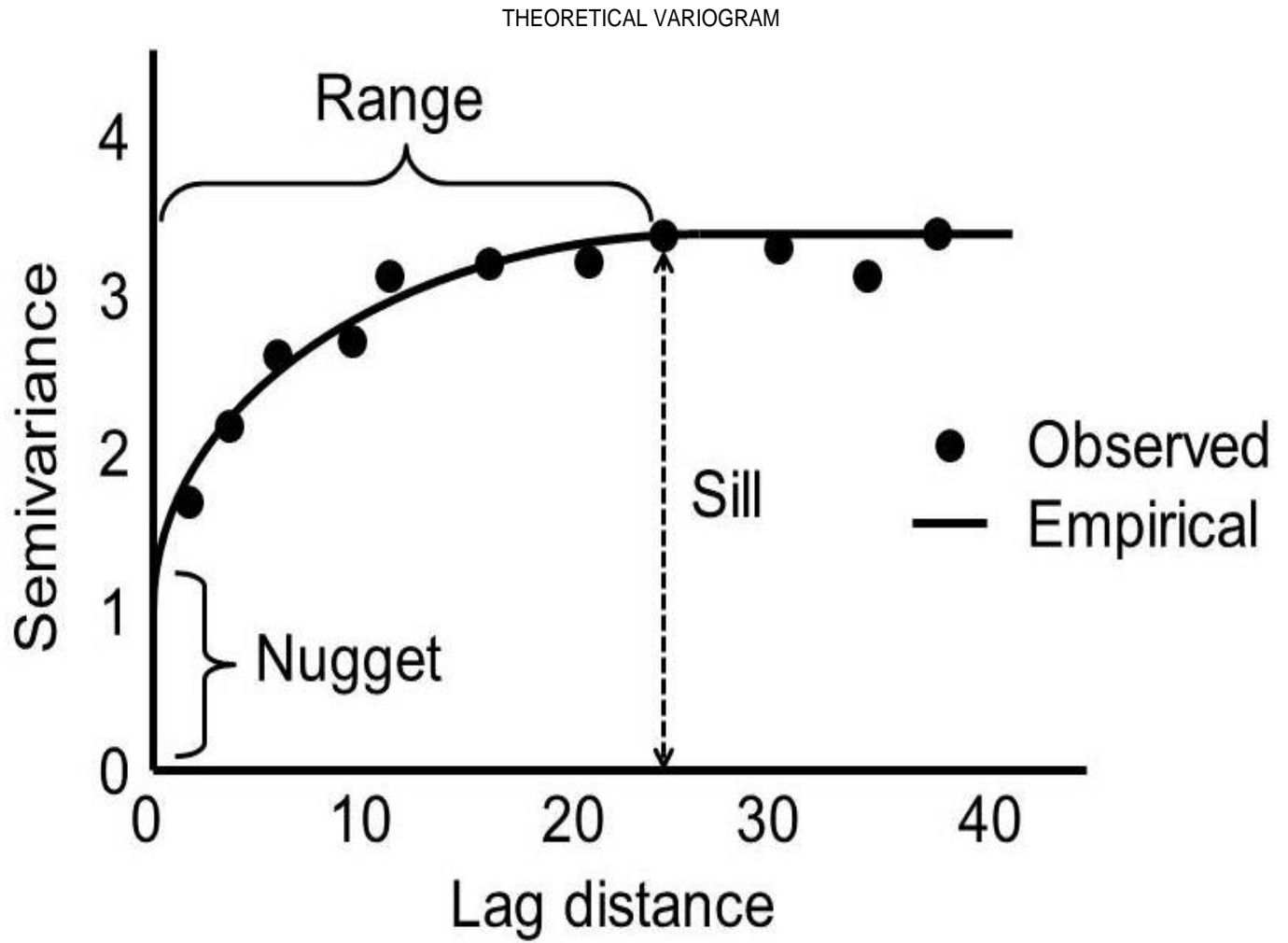
Fig. 3. The plot of a typical theoretical semivariogram.

FLOW CHART OF THE PROPOSED METHODOLOGY
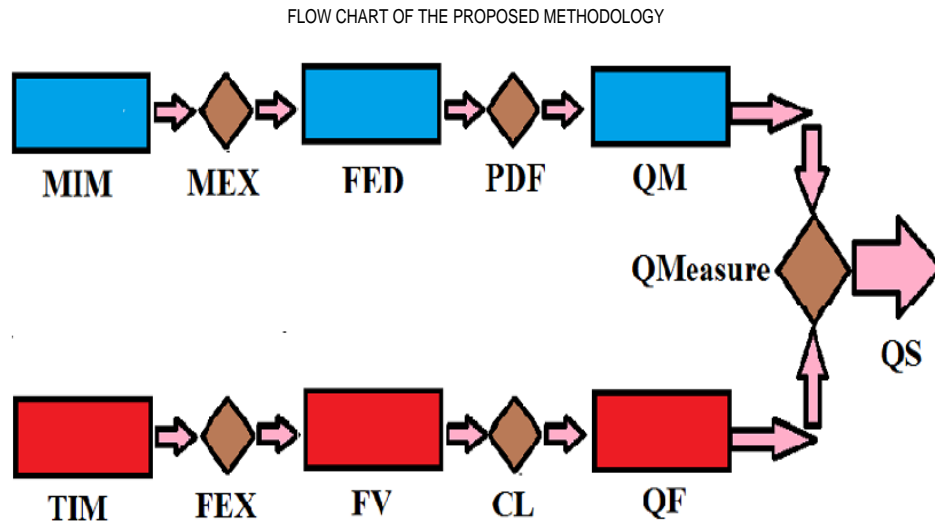
Fig. 4. The flow chart of our proposal. It begins with the use of model images **MIM** in a modeling experiment **MEX** that results in the generation of feature database **FED**. Application of classical statistics (**PDF**) on the feature database results in quality model **QM**. Given a test image **TIM**, quality feature vector **FV** is computed after feature extraction **FEX**. Quality feature **QF** is derived from feature classification **CL**. Quality score **QS** is measured **QMeasure** by normalizing quality feature **QF** with the quality model **QM**.
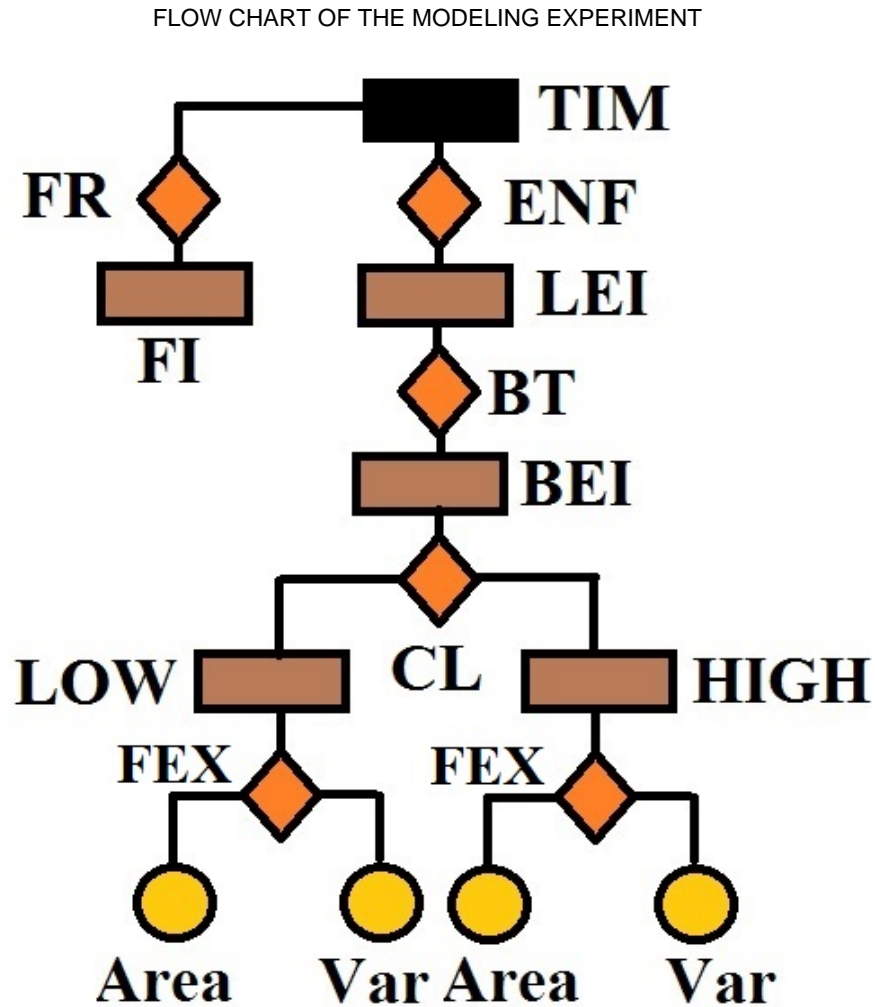
Fig. 5. Flow chart of the modeling experiment. Foreground **FI** of a model image **TIM** is extracted **FX** and the same image is fed into an entropy filter **ENF**. The local entropy image **LEI** is thresholded and transformed **BT** into a binary image **BEI**. The binary image is classified **CL** into low **LOW** and high **HIGH** entropy image. Area **Area** and semivariogram **Var** features are extracted **FEX** from each of the low and high entropy images.
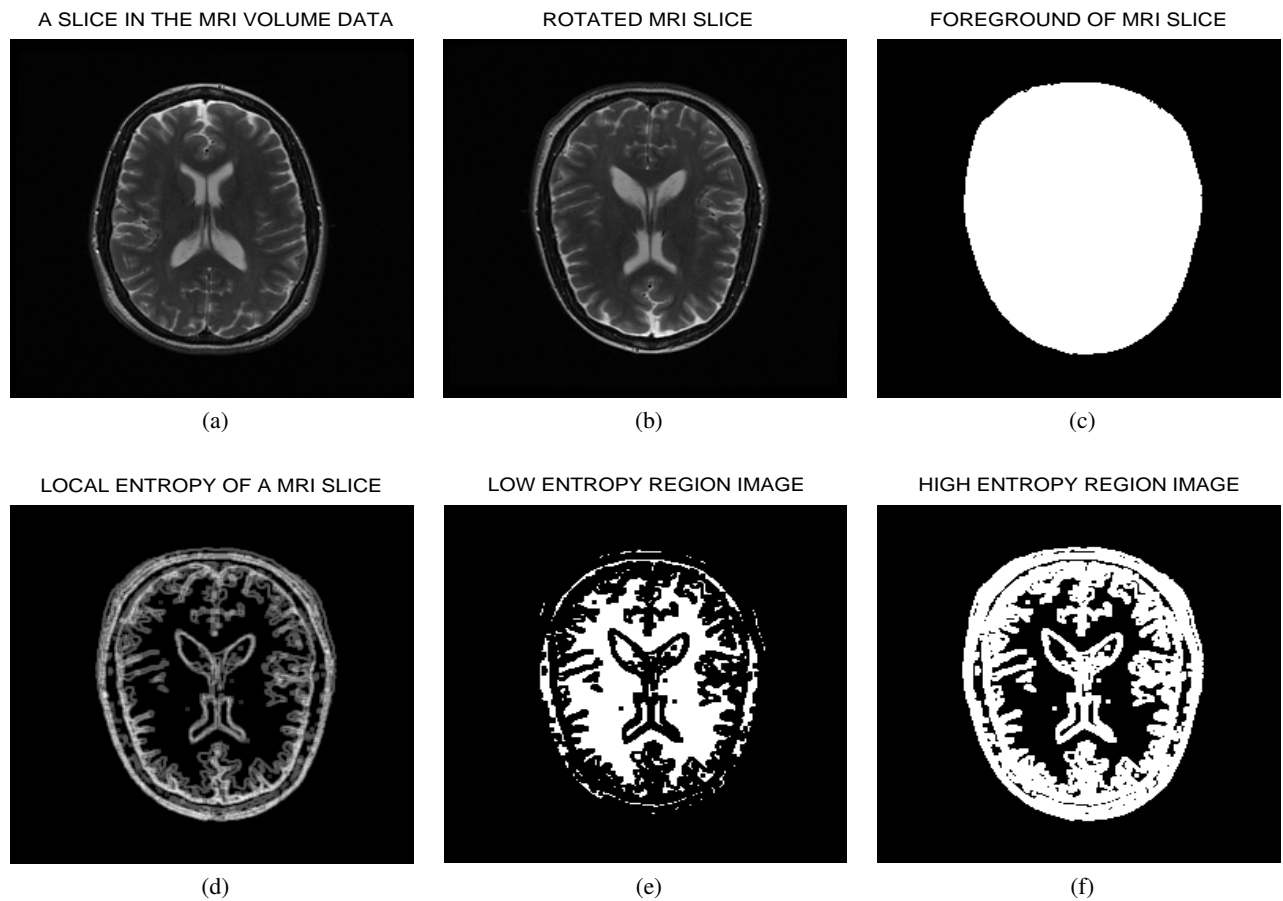
Fig. 6. In the initial steps for quality assessment the test image (a) is rotated by 180 degrees (b) to align with the model images in the database. The foreground (c) is extracted, followed by filtering to derive the local entropy image (d). The local entropy image is transformed to the binary domain to derive the low entropy image (e) and the high entropy image (f).
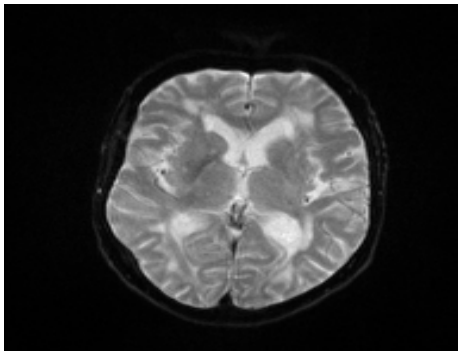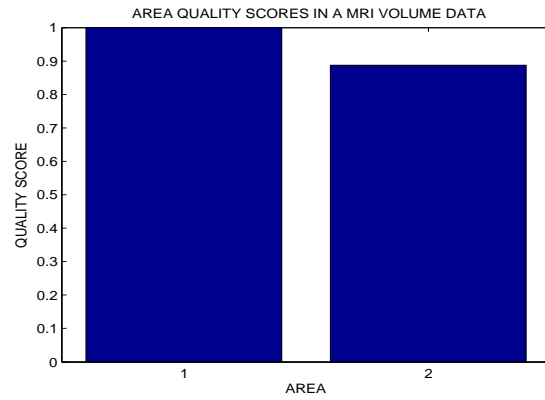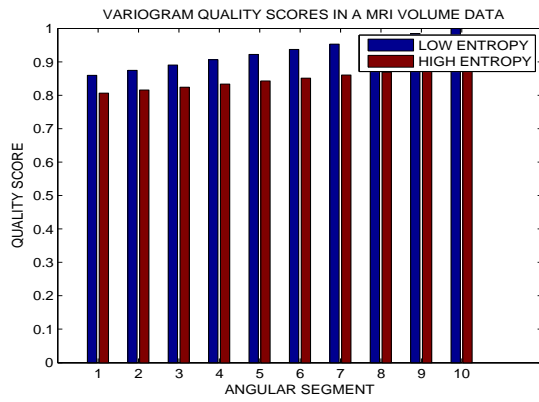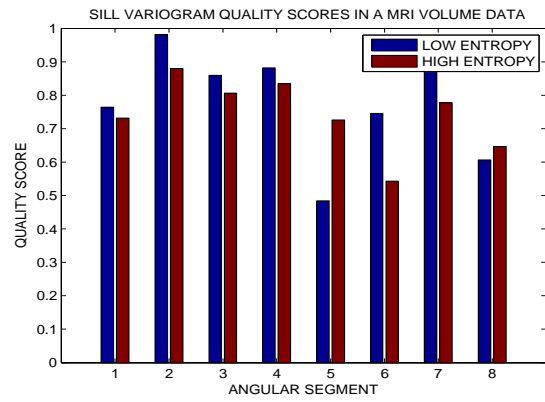
Fig. 7. A T2-weighted slice in the MRI volume data (a) from BrainCare. The area (b), semivariogram (c) and sill (d) quality scores for the low and high entropy regions of the volume data.
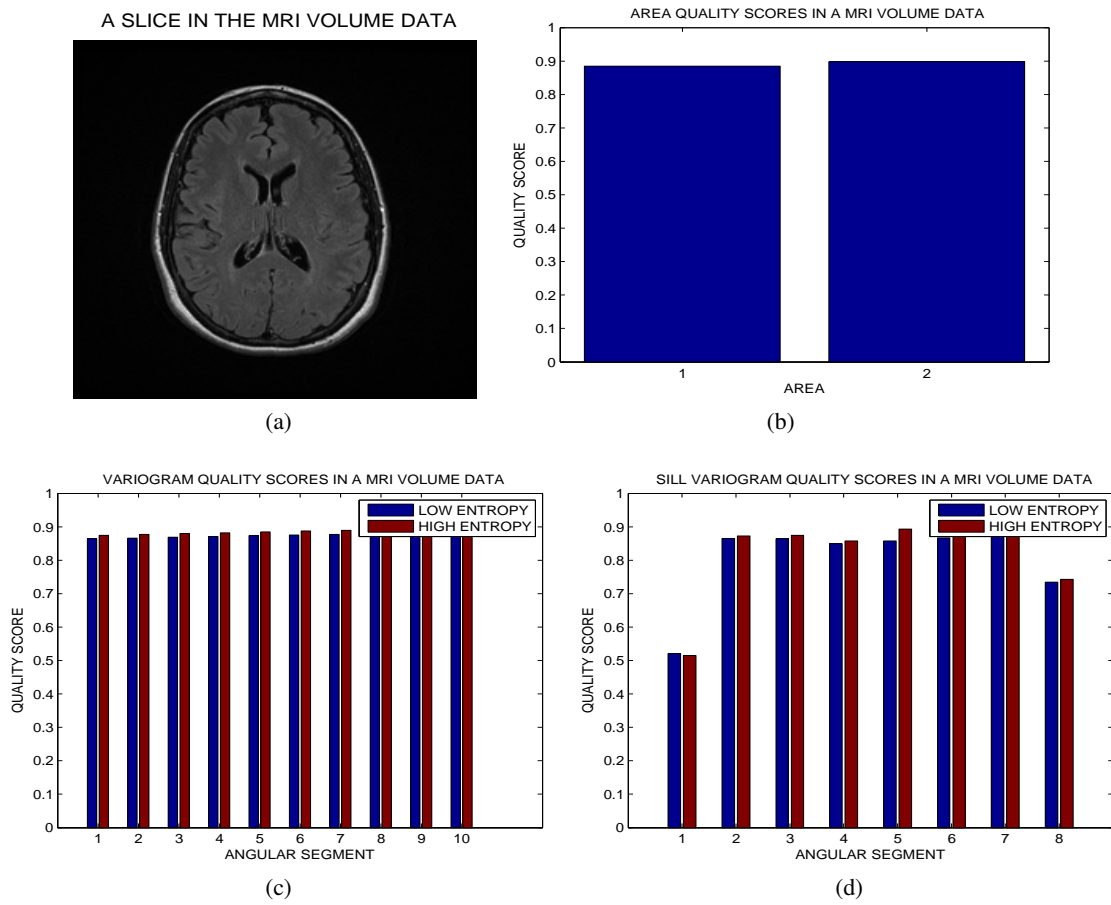
Fig. 8. A FLAIR slice in the MRI volume data (a) from NeuroRx. The area (b), semivariogram (c) and sill (d) quality scores for the low and high entropy regions of the volume data.
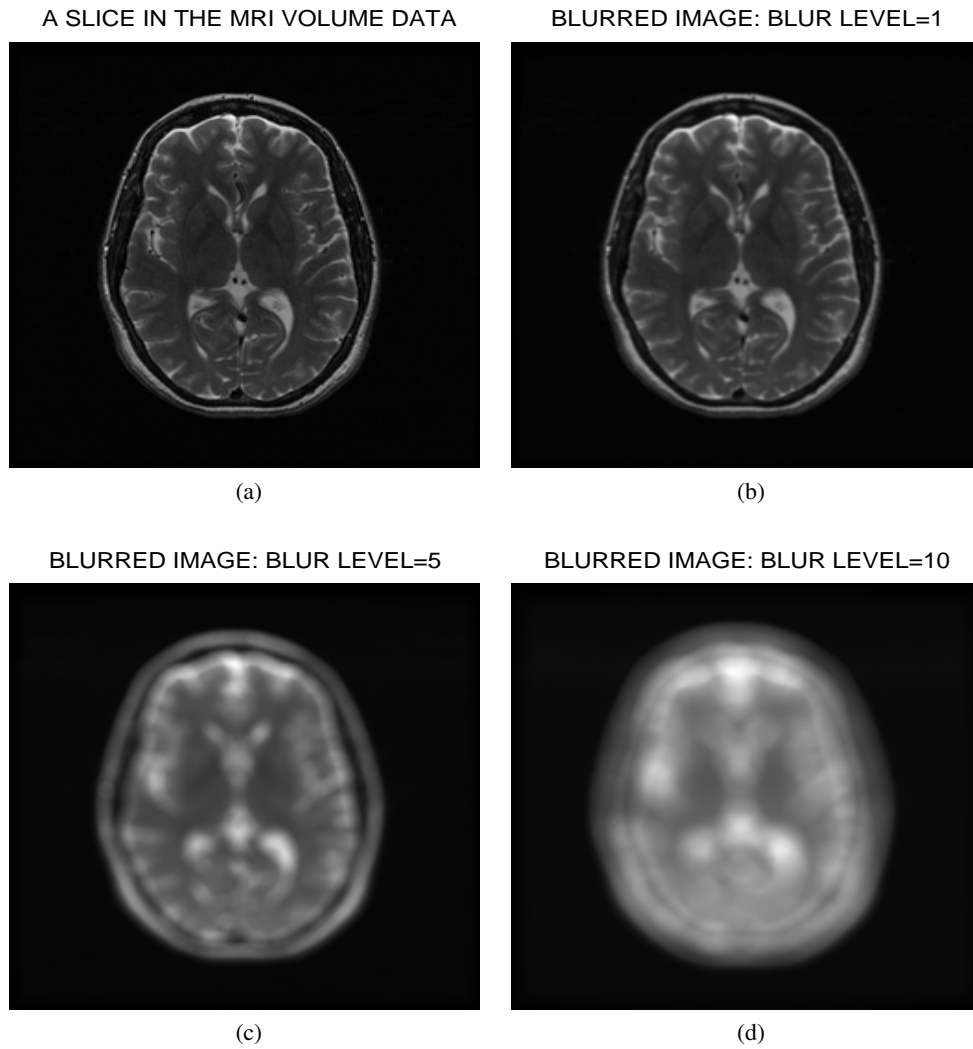
Fig. 9. A slice in the MRI volume data without blur degradation (a). The same slice in (a) with different levels of blur degradation, (b) blur level =1, (c), blur level=5 and (d) blur level=10.
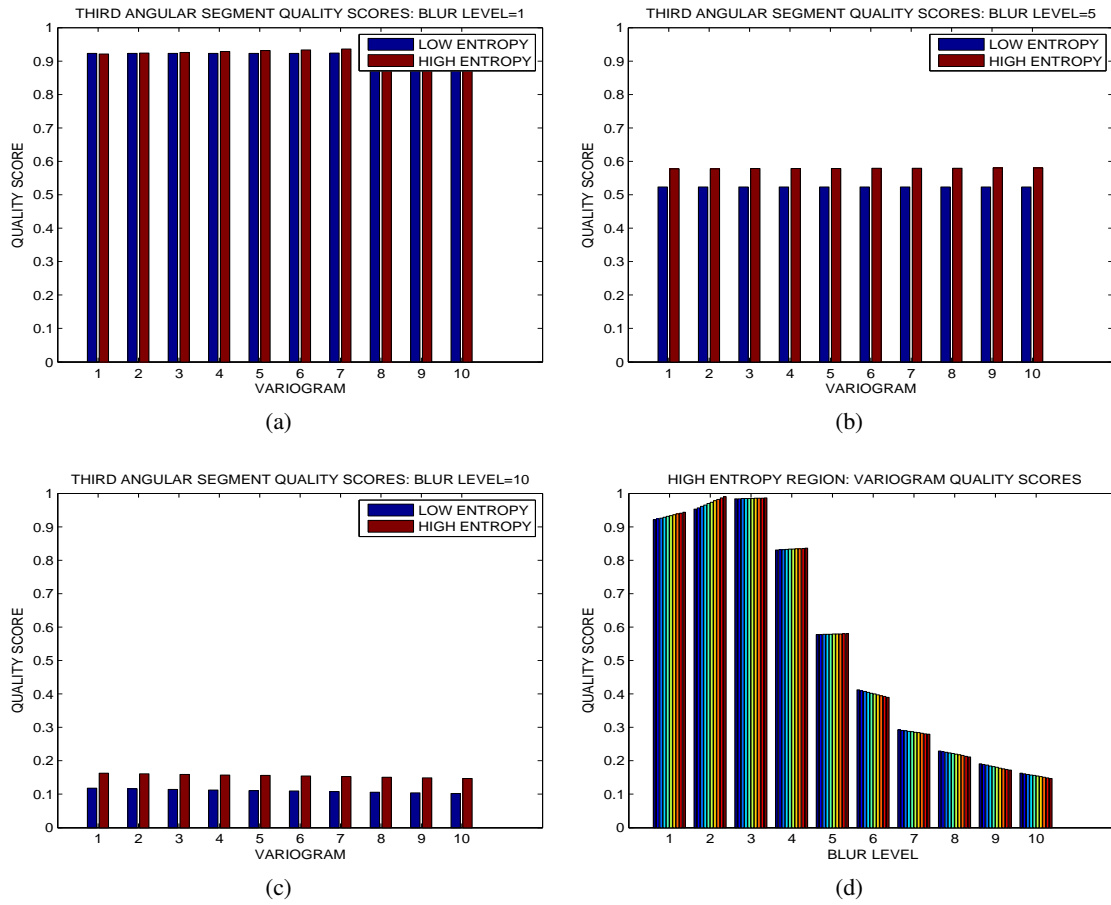
Fig. 10. The semivariogram of the MRI volume data for (a) blur level=1, (b) blur level=5, (c) blur level=10 and (d) the variation of the semivariogram with different levels of blur degradation for the third angular segment of the high entropy region.
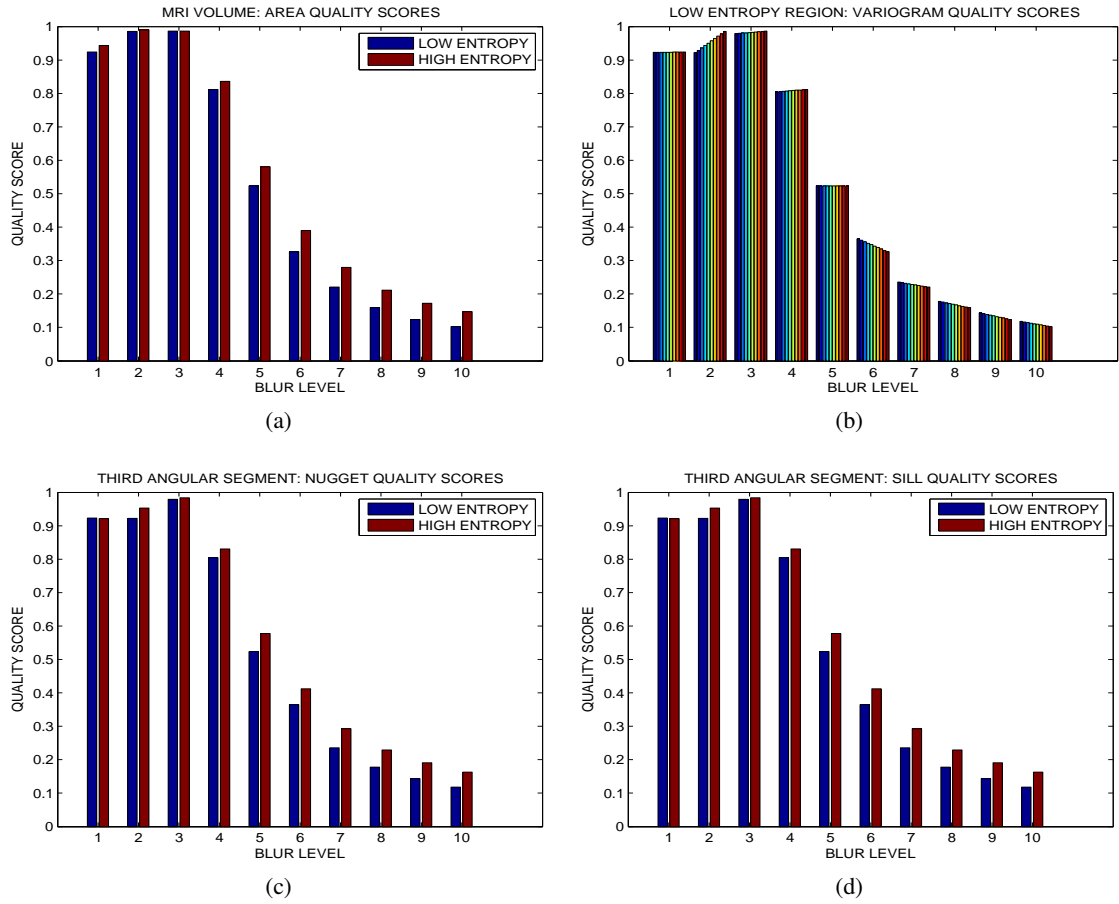
Fig. 11. Variations of the (a) area , (b) semivariogram, (c) nugget and (d) sill of MRI volume data for different levels of blur degradation.
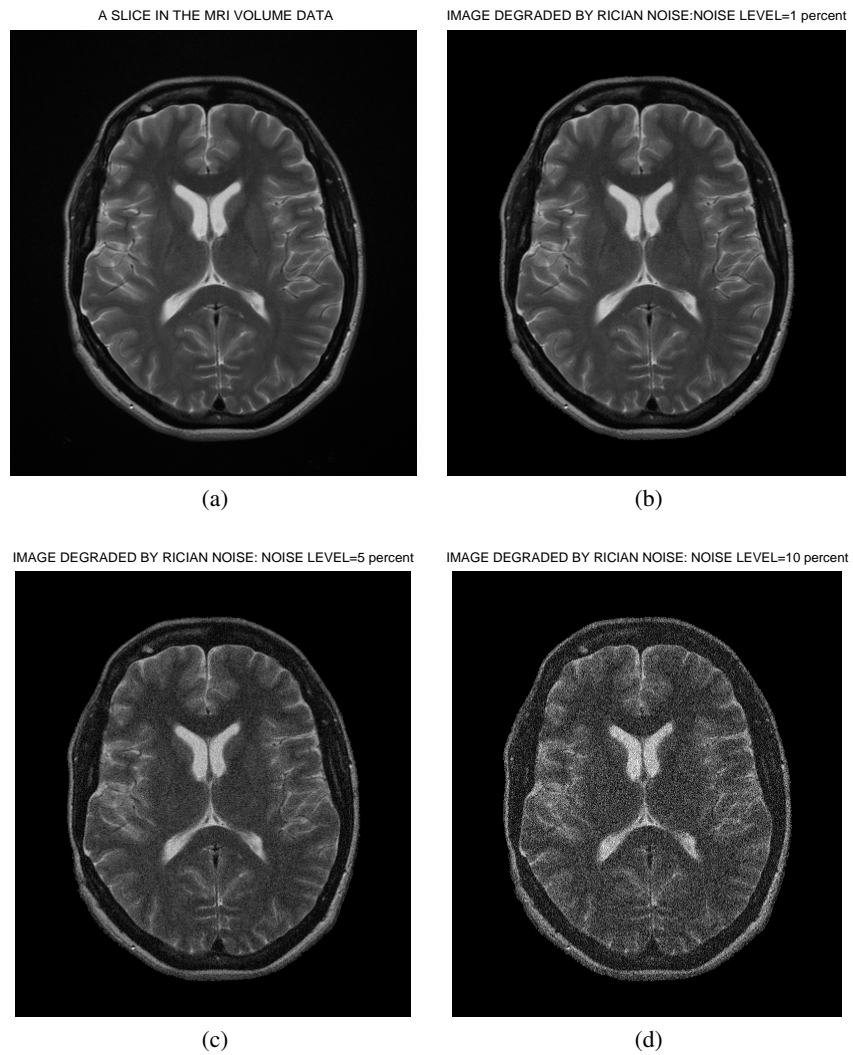
A SLICE IN THE MRI VOLUME DATA

(a)

IMAGE DEGRADED BY RICIAN NOISE:NOISE LEVEL=1 percent

(b)

IMAGE DEGRADED BY RICIAN NOISE: NOISE LEVEL=5 percent

(c)

IMAGE DEGRADED BY RICIAN NOISE: NOISE LEVEL=10 percent

(d)

Fig. 12. A slice in the MRI volume data without noise degradation (a). The same slice in (a) with different levels of noise degradation, (b) noise level =1 percent, (c), noise level=5 percent and (d) noise level=10 percent.
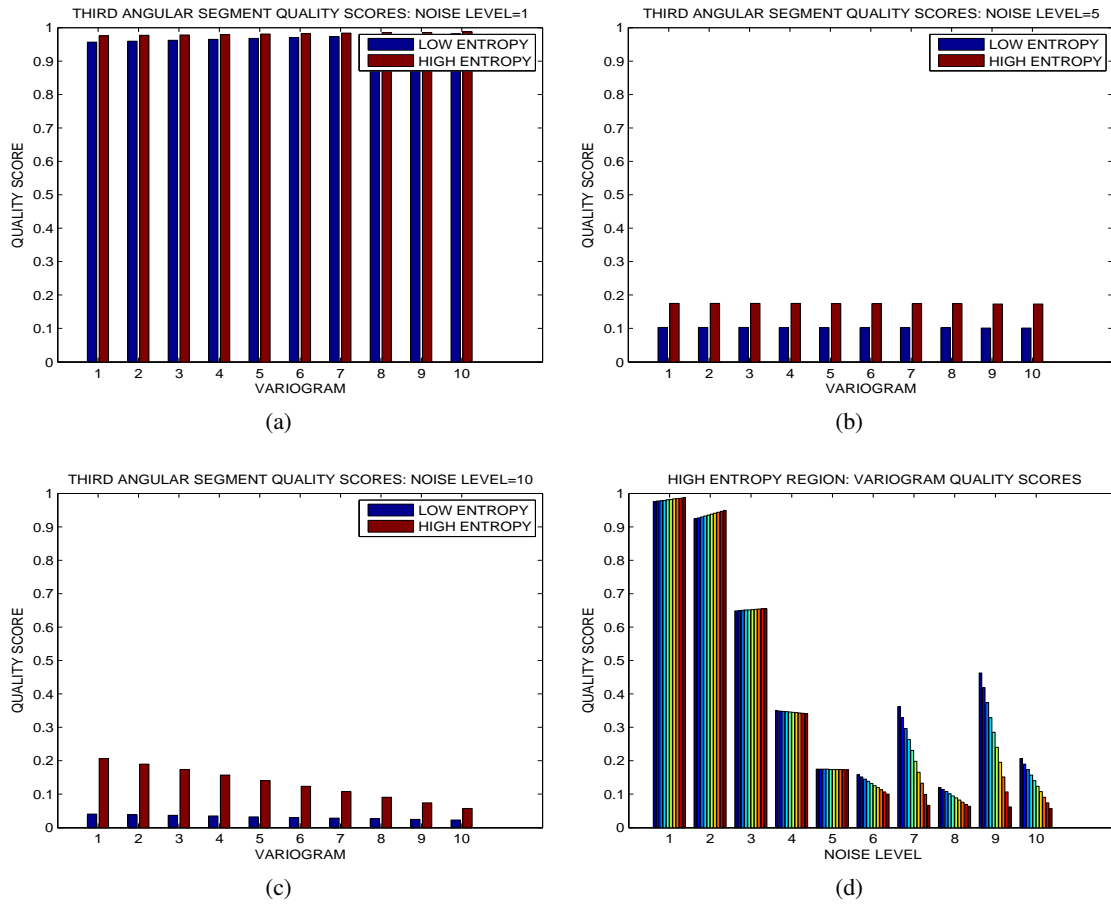
Fig. 13. The semivariogram of the MRI volume data for (a) noise level=1 percent, (b) noise level=5, (c) noise level=10 percent and (d) the variation of the semivariogram with different levels of noise degradation for the third angular segment of the high entropy region.
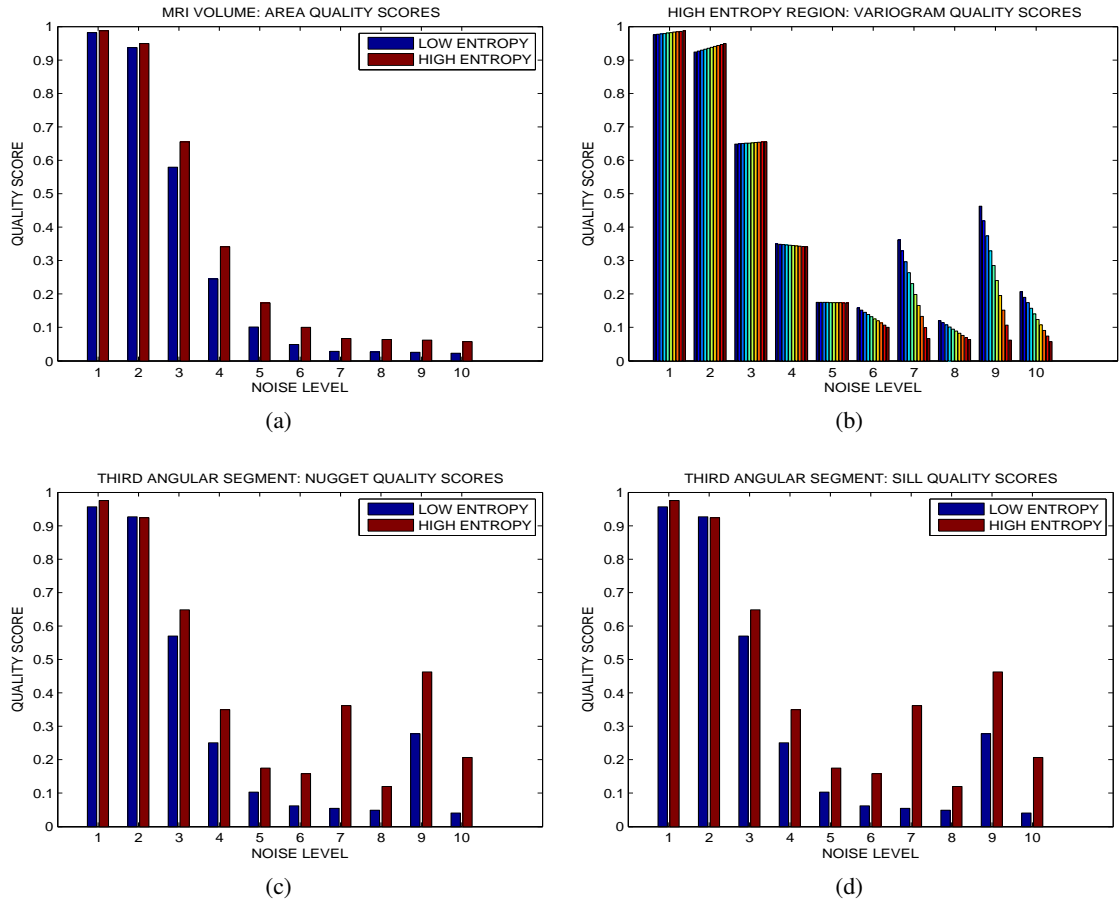
Fig. 14. Variations of the (a) area , (b) semivariogram, (c) nugget and (d) sill of MRI volume data for different levels of noise degradation.